ISSN 1674-1056
http://cpb.iphy.ac.cn
http://iopscience.iop.org/cpb
中国物理 B
Chinese Physics
中国物理 Chinese Physics B

Mechanism of defect evolution in H^+ and He^+ implanted InP

Ren-Jie Liu(刘仁杰), Jia-Jie Lin(林家杰), N Daghbouj, Jia-Liang Sun(孙嘉良), Tian-Gui You(游天桂), Peng Gao(高鹏), Nie-Feng Sun(孙聂枫), and Min Liao(廖敏)

Citation: Chin. Phys. B, 2021, 30 (**8**): 086104. DOI: 10.1088/1674-1056/abf640
Journal homepage: http://cpb.iphy.ac.cn; http://iopscience.iop.org/cpb

What follows is a list of articles you may be interested in

The formation of nano-twinned 3C-SiC grains in Fe-implanted 6H-SiC after 1500-℃ annealing

Zheng Han(韩铮), Xu Wang(王旭), Jiao Wang(王娇), Qing Liao(廖庆), Bingsheng Li(李炳生)
Chin. Phys. B, 2021, 30 (**8**): 086107. DOI: 10.1088/1674-1056/abff43

Optical spectroscopy study of damage evolution in 6H-SiC by H$_{2}^{ + }$ implantation

Yong Wang(王勇), Qing Liao(廖庆), Ming Liu(刘茗), Peng-Fei Zheng(郑鹏飞), Xinyu Gao(高新宇), Zheng Jia(贾政), Shuai Xu(徐帅), and Bing-Sheng Li(李炳生)
Chin. Phys. B, 2021, 30 (**5**): 056106. DOI: 10.1088/1674-1056/abe9a7

Evolution of ion-irradiated point defect concentration by cluster dynamics simulation

Shuaishuai Feng(冯帅帅), Shasha Lv(吕沙沙), Liang Chen(陈良), and Zhengcao Li(李正操)
Chin. Phys. B, 2021, 30 (**5**): 056105. DOI: 10.1088/1674-1056/abf102

Defects and electrical properties in Al-implanted 4H-SiC after activation annealing

Yi-Dan Tang(汤益丹), Xin-Yu Liu(刘新宇), Zheng-Dong Zhou(周正东), Yun Bai(白云), Cheng-Zhan Li(李诚瞻)
Chin. Phys. B, 2019, 28 (**10**): 106101. DOI: 10.1088/1674-1056/ab3cc2

Structural and electrical properties of carbon-ion-implanted ultrananocrystalline diamond films

Hui Xu(徐辉), Jian-Jun Liu(刘建军), Hai-Tao Ye(叶海涛), D J Coathup, A V Khomich, Xiao-Jun Hu(胡晓君)
Chin. Phys. B, 2018, 27 (**9**): 096104. DOI: 10.1088/1674-1056/27/9/096104

SPECIAL TOPIC — Ion beam modification of materials and applications

Mechanism of defect evolution in H^+ and He^+ implanted InP*

Ren-Jie Liu(刘仁杰)[1,2,†], Jia-Jie Lin(林家杰)[3,4,†‡], N Daghbouj[5], Jia-Liang Sun(孙嘉良)[3,6], Tian-Gui You(游天桂)[3,§], Peng Gao(高鹏)[7], Nie-Feng Sun(孙聂枫)[4,8], and Min Liao(廖敏)[1,2]

[1] *Key Laboratory of Low Dimensional Materials and Application Technology of Ministry of Education, School of Materials Science and Engineering, Xiangtan University, Xiangtan* 411105, *China*

[2] *Hunan Provincial Key Laboratory of Thin Film Materials and Devices, School of Materials Science and Engineering, Xiangtan University, Xiangtan* 411105, *China*

[3] *State Key Laboratory of Functional Materials for Informatics, Shanghai Institute of Microsystem and Information Technology, Chinese Academy of Sciences, Shanghai* 200050, *China*

[4] *China Nanhu Academy of Electronics and Information Technology, Jiaxing* 314000, *China*

[5] *Department of Control Engineering, Faculty of Electrical Engineering, Czech Technical University in Prague, Technická* 2, 16000 *Prague* 6, *Czechia*

[6] *Center of Materials Science and Optoelectronics Engineering, University of Chinese Academy of Sciences, Beijing* 100049, *China*

[7] *Science and Technology on Power Sources Laboratory, Tianjin Institute of Power Sources, Tianjin* 300384, *China*

[8] *The* 13*th Research Institute, CETC, Shijiazhuang* 050051, *China*

(Received 26 January 2021; revised manuscript received 10 March 2021; accepted manuscript online 9 April 2021)

The defect evolution in InP with the 75 keV H^+ and 115 keV He^+ implantation at room temperature after subsequent annealing has been investigated in detail. With the same ion implantation fluence, the He^+ implantation caused much broader damage distribution accompanied by much higher out-of-plane strain with respect to the H^+ implanted InP. After annealing, the H^+ implanted InP did not show any blistering or exfoliation on the surface even at the high fluence and the H_2 molecules were stored in the heterogeneously oriented platelet defects. However, the He molecules were stored into the large bubbles which relaxed toward the free surface, creating blisters at the high fluence.

Keywords: ion implantation, defect evolution, ion-slicing, damaged band

PACS: 61.72.−y, 61.72.Cc, 61.80.Jh, 61.82.Fk **DOI:** 10.1088/1674-1056/abf640

1. Introduction

Heterogeneous integration of InP with Si has drawn considerable attention because of its excellent ability to achieve the monolithic integration of the mature Si-based circuits with the InP-based optoelectronics.[1–4] It is difficult to heteroepitaxially grow the high-quality thin InP layer on the Si-based substrate because of the large lattice mismatch (8% mismatch), different polarity, and different thermal expansion coefficients (73.1% mismatch).[5,6] Generally, a large density of defects, such as threading dislocations and antiphase boundaries will be introduced in the epitaxial InP layer. Alternatively, the ion-slicing technology via the H^+ or He^+ implantation and layer splitting can transfer the high-quality thin layers onto the mismatched substrates without any physical mismatched problems in the epitaxial process.[7–10]

The ion-slicing technology, commercially known as Smart-Cut^{TM}, was developed by Bruel in 1995 and has been commercially applied to produce 12-inch Si-on-insulator (SOI) wafers.[11] In this technique, the defects introduced by the H^+ and He^+ implantation agglomerate into overpressurized microcracks during annealing, which could cause the layer splitting process. When the H^+ or He^+ implanted wafer is bonded to a foreign substrate as a stiffener, the layer will split parallelly to the bonding interface.[12–14] However, this process can only occur in the defined parameter windows, including ion species, ion fluence, and annealing temperature, because the splitting process strongly depends on the materials. Generally, the H^+ or He^+ implanted wafers before bonding are used to investigate the defect evolution and reveal the physical mechanism of ion-slicing technique.[15–17] The exfoliation process of the InP caused by the H^+ or He^+ implantation at a narrow temperature window was previously reported. With the H^+ implantation, the blistering or exfoliation on the InP surface could only be achieved in the two narrow implantation temperature windows (i.e., 150 °C to 250 °C and −20 °C to 20 °C).[18,19] For the He^+ implantation, the InP layer could only be transferred to a Si substrate in a distinct implantation temperature (−15 °C or 20 °C).[20] Our earlier investigation

*Project supported by the National Key R&D Program of China (Grant No. 2017YFE0131300), the National Natural Science Foundation of China (Grant Nos. 61874128, 61851406, and 11705262), Frontier Science Key Program of Chinese Academy of Sciences (Grant Nos. QYZDY-SSW-JSC032 and ZDBS-LY-JSC009), Chinese–Austrian Cooperative R&D Project (Grant No. GJHZ201950), Program of Shanghai Academic Research Leader (Grant No. 19XD1404600), K. C. Wong Education Foundation (Grant No. GJTD-2019-11), and NCBiR within the Polish–China (Grant No. WPC/130/NIR-Si/2018).

†These authors contributed equally.

‡Corresponding author. E-mail: jjlin@mail.sim.ac.cn

§Corresponding author. E-mail: t.you@mail.sim.ac.cn

© 2021 Chinese Physical Society and IOP Publishing Ltd

has shown the efficient exfoliation of the InP layer by the co-implantation of He^+ and H^+ at room temperature.[17] However, the defect evolution in the InP wafer implanted with the H^+ and He^+ at room temperature has not been investigated in detail.

In this study, we will present the microstructure evolution upon the He^+ and H^+ implanted InP at room temperature before and after subsequent annealing. Based on the detailed investigation of the underlying mechanism of the defect formation, the reasons for the absence and the presence of the blisters will be clarified.

2. Experimental details

The 2-inch semi-insulating (100) InP wafers were used in this study. The H^+ or He^+ implantation was carried out on the InP wafers at room temperature, respectively. During implantation, the surface normal to the sample was tilted at an angle of 7° with respect to the ion beam direction in order to avoid channeling effects. The H^+ and He^+ energies were taken as 75 keV and 115 keV, respectively, in order to obtain the similar ion stopping range (R_p) in the InP. Both fluences of H^+ and He^+ were 2×1^{16} cm^{-2}, 5×1^{16} cm^{-2} and 1×1^{17} cm^{-2}. The implanted InP wafers were cut into small samples with a size of 10 mm × 10 mm. Some of the as-implanted samples were isothermally annealed at 300 °C under a constant flux of N_2. The optical microscope (OM), Leica DM4000M, was performed to characterize the surfaces of wafers. The strain introduced by the ion implantation was characterized by the x-ray diffraction (HXRD) with Philips X'Pert x-ray diffractometer. The defects created by ion implantation in the InP wafers after annealing were investigated by the cross-sectional transmission electron microscopy (XTEM) with a JEOL 2100F field-emission transmission electron microscope, in which the samples were prepared by thinning to the electron transparency using standard focused ion beam (FIB) milling procedures in the Helions Nanolab 600 workstation.

3. Results and discussion

As the Stopping and the Range of Ion in Matter (SRIM) calculations[21] with the displacement energy of 4 eV and 8 eV for In and P sublattices,[22] and a density of 4.81 g/cm^3 for the InP, the H^+ and He^+ depth distributions and the damage of displacement per atom (DPA) distributions are shown in Fig. 1. The Rp of H^+ is almost consistent with that of He^+, approximately 630 nm, as shown in Fig. 1(a). However, the full width at the half maximum (FWHM) (321 nm) of the He^+ distribution profile is much larger than that (207 nm) of the H^+ distribution profile. In addition, the concentration of H^+ is about 1.6 times larger than that of He^+ at R_p and the H^+ shows more concentrated distribution. Figure 1(b) shows the SRIM-calculated damage profiles of the DPA in InP which are calculated via using the following equation:

$$\mathrm{DPA} = D\varphi/\rho_{\mathrm{at}}, \tag{1}$$

where D is the number of total displacements (the sum of In vacancies, P vacancies and replacement collisions events) per unit length, φ is the total fluence, and ρ_{at} is the atomic number density of the material. The maximum damage depth for the H^+ and He^+ implantation is similar around 560 nm from the surface which is shallower than the peak ion concentration ($\sim 89\%\ R_p$). The He ions create much more defects than the H ions which is manifested in the value of the He^+ peak damage of 5.5 DPA, while the H^+ peak damage is around 0.44 DPA.

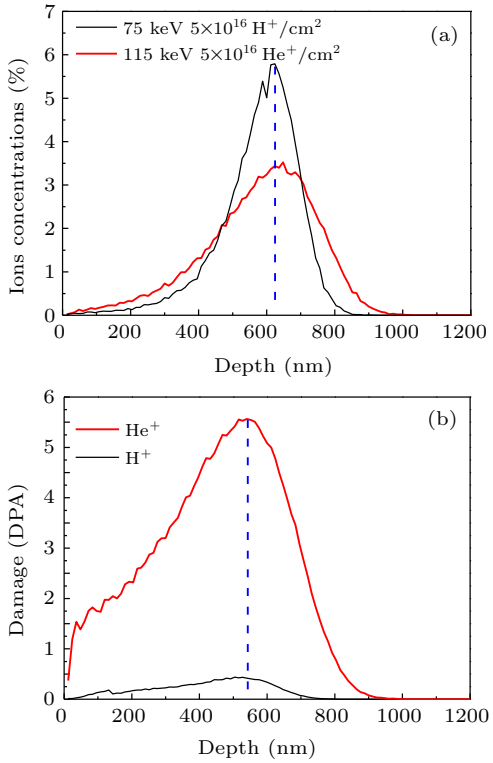


Fig. 1. (a) The H^+ and He^+ depth profiles and (b) the H^+ and He^+ implantation-introduced damage profiles of DPA simulated by SRIM 2008.[21]

In order to determine the out-of-plane strain created by the ion implantation, the InP samples implanted with the H^+ and He^+ fluence of 5×1^{16} cm^{-2} were performed by the XRD. Figure 2(a) shows the $\omega/2\theta$ scan XRD curves in the vicinity of the (004) reflections of InP. It is obvious that there are many additional scattered fringe patterns at the lower-angle side of the Bragg angle. It means that the InP lattice in the ion-implanted layer is expanded, which is manifested by the out-of-plane positive strain gradient.[23] The periodicity of the fringe and lowest-angle fringe characterize the width of the strain layer and the maximum strain in the InP samples, respectively. It is also obvious that the fringe spacing for the He^+ implantation is smaller than that for the H^+ implantation, which indicates a broader strain profile. Moreover, the lower

scattered intensity for the He^+ implantation is indicative of the higher disorder.[23] The strain distribution can be extracted by fitting the XRD patterns basing on the dynamical theory of x-ray diffraction in a web-based program GID_SL.[24] It is reasonable to assume that the lattice strain is proportional to the He^+ and H^+ concentrations and the out-of-plane strain follows the ion profile given in Fig. 1(a). The damaged band is divided into many adjustable strain sublayers with the given thickness. The good fit with the experimental curves can be achieved by gradually modifying the simulated HR-XRD curves.[25] The simulated HR-XRD pattern approaches the experimental data well as shown in Figs. 2(b) and 2(c). Based on the simulation, the strain distribution is shown in Fig. 2(d). Both strain profiles show Gaussian-like distributions and reach the maximum values of 1.1% for the H^+ implantation and 1.8% for the He^+ implantation, respectively, around the peak region of the R_p. Although the strain profiles for both ion implantations show a similar distribution width, the He^+ implantation introduced a much larger strain gradient. As the previous report, the out-of-plane strain introduced by the ion implantation is the driving force of the nucleation and growth of defects.[26] Moreover, the coalescence of the platelets to form microcracks is driven by the relaxation of the stress (out-of-plane strain).[27] Hence, benefiting from the large strain gradient, the He^+ implantation may be more effective to achieve the blistering or exfoliation on the surface of the InP.

After the implantation of He^+ and H^+ with fluence of 2×1^{16} cm^{-2}, 5×1^{16} cm^{-2}, and 1×1^{17} cm^{-2} at room temperature, respectively, there was no blister formation on the surface of the implanted InP (not shown here). In order to check whether it is possible to obtain the surface blisters after post-annealing, the as-implanted samples were annealed at 300 °C in a flowing N_2 ambient. The variations of surface morphology as the ion fluence and ion species were illustrated by the OM images in Fig. 3. In the case of H^+ implantation, there was no blister or exfoliation observed on the InP surface even when the H^+ fluence reached 1×1^{17} cm^{-2}, as shown in Fig. 3(a). This phenomenon is in agreement with the results in the previous reports, in which only two distinct H^+ implantation temperature ranges (i.e., 150 °C to 250 °C and −20 °C to 20 °C) can potentially lead blistering or exfoliation on the surface of InP after annealing.[18,19,28] The implantation temperature is the primary influence factor for the H^+ implantation to achieve the InP layer transfer. In the case of He^+ implantation, with the fluence below 5×1^{16} cm^{-2}, no blister or exfoliation was observed on the surface as shown in Fig. 3(b). However, by further increasing the He^+ fluence to 1×1^{17} cm^{-2}, a large density of blisters appears uniformly on the surface, as shown in Fig. 3(b). Previously, the blisters on the surface of InP with the low He^+ implantation fluence (5×1^{16} cm^{-2}) can be achieved only at the low implantation temperature (−15 °C or 20 °C).[20] It is well known that the implantation temperature is very hard to be controlled due to its high sensitivity to the mode of clamping the wafer to the chuck and the ion flux. Hence, InP layer transfer by the He^+ implantation at room temperature is promising to be achieved at higher fluence of He^+ instead of the low implantation temperature.

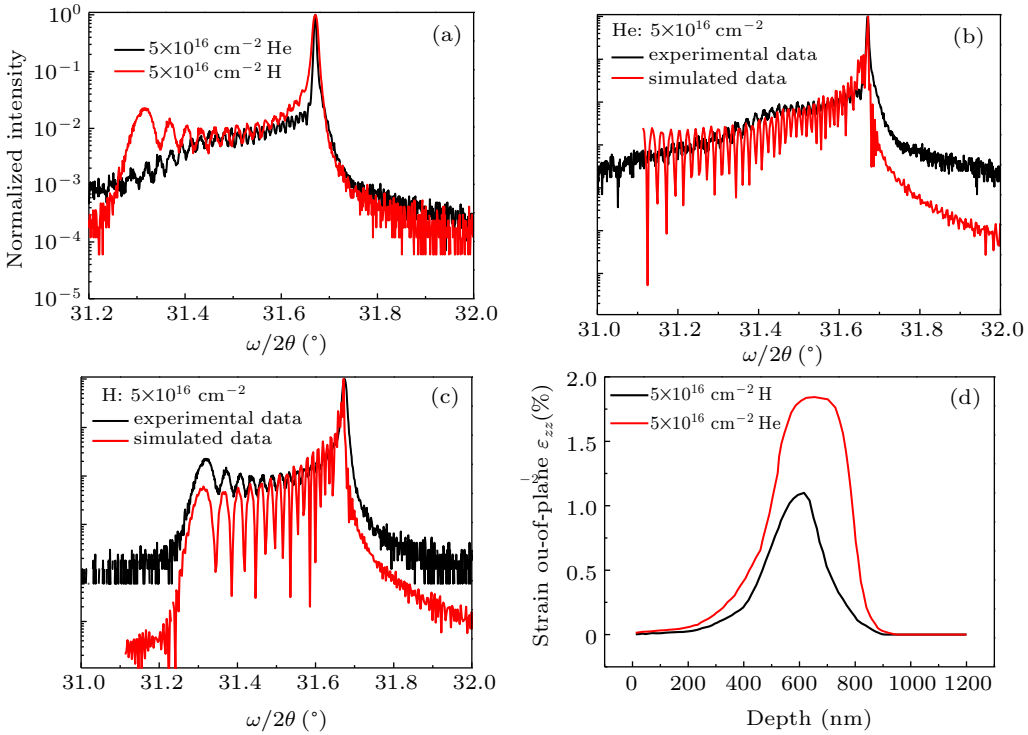


Fig. 2. (a) The $\omega/2\theta$ scan XRD curves along the InP (004) reflection for InP implanted with 5×10^{16} cm^{-2} H^+ and He^+. (b) and (c) The simulated and the experimental HR-XRD patterns. (d) The simulated out-of-plane strain profiles.

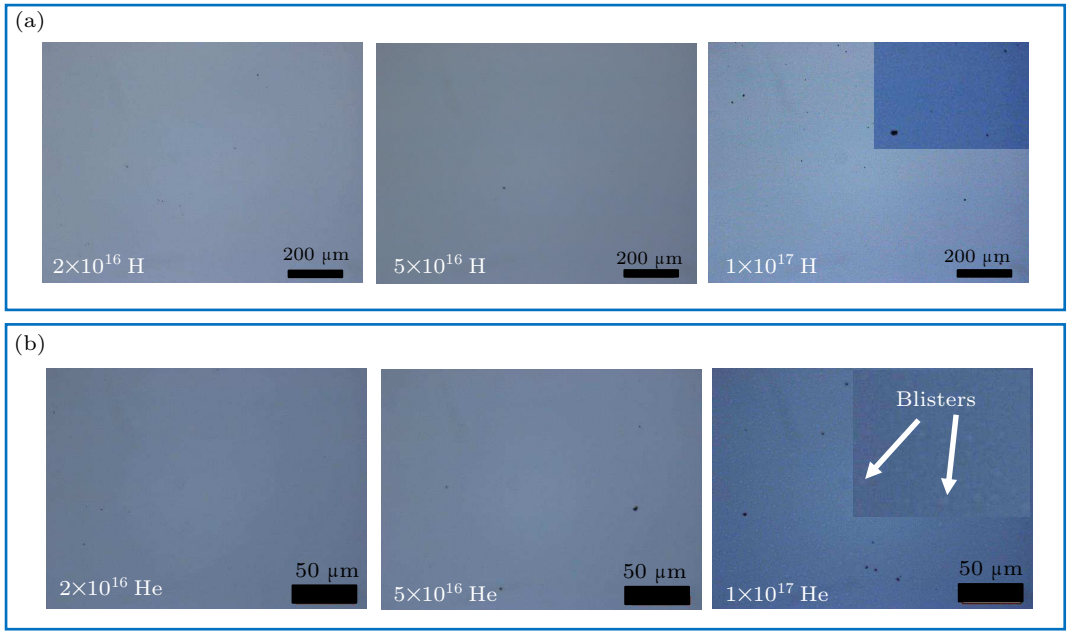


Fig. 3. The OM images of InP implanted with 2×10^{16} cm^{-2}, 5×10^{16} cm^{-2}, 1×10^{17} cm^{-2} (a) H^+ and (b) He^+ after annealing at 300 °C for 1 h.

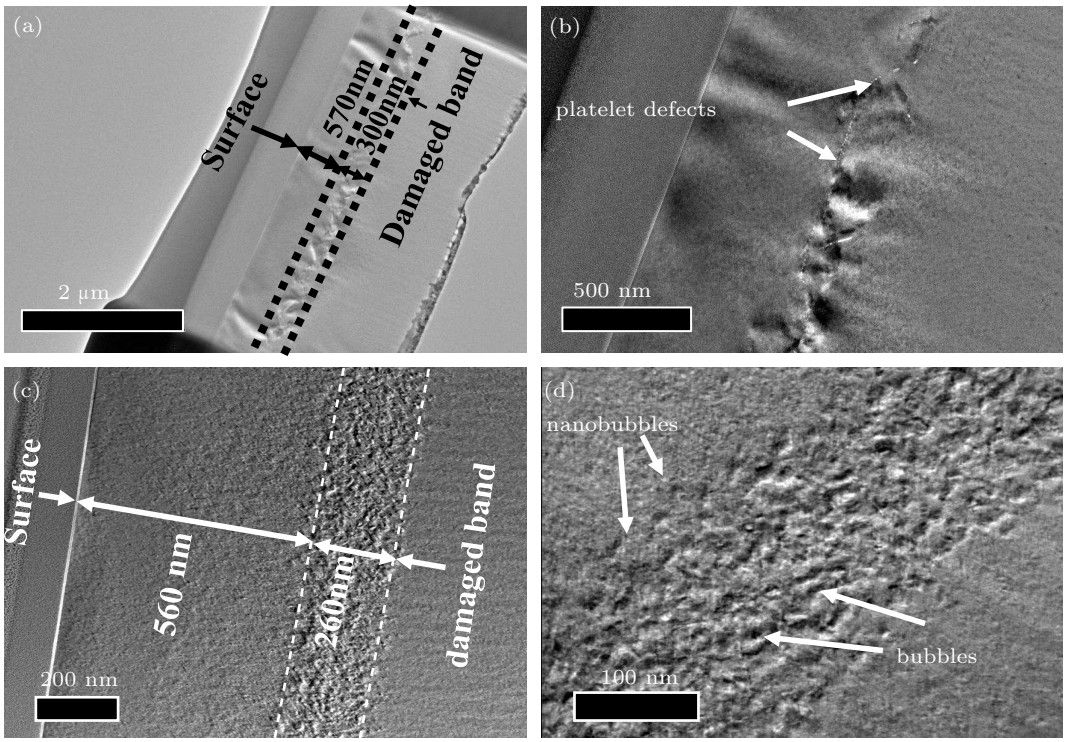


Fig. 4. The XTEM images of the InP: (a) the 5×10^{16} cm^{-2} H^+ implanted sample annealed at 300 °C for 1 h; (b) an amplified image of the damaged band in (a); (c) the 5×10^{16} cm^{-2} He^+ implanted sample annealed at 300 °C for 1 h; (d) an amplified image of the damaged band in (c).

To understand the different behaviors of the He^+ and H^+ inside InP matrix after annealing, we analyzed the microstructure via the XTEM. The H^+ implantation with subsequent annealing at 300 °C for 1 h, introduced a damaged band consisting of a large density of defects in the InP sample, as shown in Fig. 4(a). The damaged band extends approximately to 300 nm width and is located at 570 nm from the surface of the InP wafer. The higher magnification XTEM image of the damaged band is shown in Fig. 4(b), which clearly shows a small number of platelet defects approaching the upper boundary of the damaged band. These platelet defects are two dimensional discs which results from the co-precipitation of vacancies and hydrogens, with internal surfaces passivated by hydrogen and internal space filled with H_2 molecules under high pressure. However, the large concentration of platelet defects is inclined at arbitrary angles with respect to the (001) surface with few (001) oriented platelet defects and these platelet defects' orientations are related to the strain magnitude.[29]

The more platelet defects are well oriented (parallel to the surface), the more likely the cleavage occurs. As shown in Fig. 4(c), the He^+ implantation also introduces a damaged band at the depth of 560 nm corresponding to the maximum damaged depth simulated by SRIM in Fig. 1(a). The damaged band extends to about 260 nm, which is much smaller than that introduced by the H^+ implantation. In the higher magnification XTEM image of the damaged band shown in Fig. 4(d), it can be found that a large number of bubbles distribute through the entire damaged band with a small number of nanobubbles around the upper boundary, which is quite different from the defects introduced by the H^+ implantation. As the previous reports, the He^+ implantation could create a large number of spherical nanobubbles with a diameter of a few nanometers.[12,30] During annealing, the nanobubbles agglomerate via Ostwald ripening (diffusion of vacancies and He gas from the small ones to the large ones) and assist in the formation of the large bubbles.[29] Then when the density of bubbles is higher enough and the distance between bubbles is small enough (overlap of strain field), coalescence between bubbles will occur and then the large cavities will form. These cavities which are pressurized by He gas, relax to the free surface and create blisters on the surface.[31] So, at the 1×10^{17} He^+/cm^2 and after annealing at 300 °C for 1 h, the He atoms and vacancies can diffuse locally to form bubbles, and the InP matrix stored enough strain to make the coalescence of the bubbles favorable. Hence, the He^+ ion implantation at this condition is more efficient to split the InP layer from the InP wafer than the H^+ implantation.

4. Conclusion

A detailed investigation about the mechanism of defect evolution in the InP implanted with the H^+ and He^+ at room temperature was carried out. Compared with the H^+ implantation, the He^+ implantation introduced a much broader FWHM of the distribution profile and more damage in the InP even with the same ion fluence. Additionally, the larger strain gradient caused by the He^+ implantation is favorable for the defect migration. After annealing, although there are few platelet defects in the damaged band of the H^+ implanted InP, the blisters and exfoliation do not form due to the arbitrary angles of the platelet defects. In contrast, the He^+ implantation could introduce more concentrated bubbles. By increasing the ion fluence to 1×1^{17} He^+/cm^2, the blisters appeared on the surface. Hence, it is promising to achieve the InP layer transfer by the He^+ implantation with the higher fluence at room temperature.

References

[1] Thiessen T, Grosse P, Fonseca J Da, Billondeau P, Szelag B, Jany C, Poon J k S and Menezo S 2019 *Opt. Express* **27** 102

[2] Kazior T E, LaRoche J R, Lubyshev D, Fastenau J M, Liu W K, Urteaga M, Ha W, Bergman J, Choe M J, Bulsara M T, Fitzgerald E A, Smith D, Clark D, Thompson R, Drazek C, Daval N, Benaissa L and Augendre E 2009 *IEEE MTT-S International Microwave Symposium Digest* p. 1113

[3] Abbasi A, Verbist J, Shiramin L A, Verplaetse M, De Keulenaer T, Vaernewyck R, Pierco R, Vyncke A, Yin X, Torfs G, Morthier G, Bauwelinck J and Roelkens G 2018 *IEEE Photon. Technol. Lett.* **30** 1095

[4] Pintus P, Zhang Z, Pinna S, Tran M A, Jain A, Kennedy M J, Ranzani L, Soltani M and Bowers J E 2019 *APL Photon.* **4** 100805

[5] Lee S M, Cho Y J, Park J B, Shin K W, Hwang E, Lee S, Lee M J, Cho S H, Su Shin D, Park J and Yoon E 2015 *J. Cryst. Growth* **416** 113

[6] Moutanabbir O and Gösele U 2010 *Annu. Rev. Mater. Res.* **40** 469

[7] Yi A, Zheng Y, Huang H, Lin J, Yan Y, You T, Huang K, Zhang S, Shen C, Zhou M, Huang W, Zhang J, Zhou S, Ou H and Ou X 2020 *Opt. Mater. (Amst).* **107** 109990

[8] Shi H, Huang K, Mu F, You T, Ren Q, Lin J, Xu W, Jin T, Huang H, Yi A, Zhang S, Li Z, Zhou M, Wang J, Xu K and Ou X 2020 *Semicond. Sci. Technol.* **35** 125004

[9] Lin J, You T, Jin T, Liang H, Wan W, Huang, H, Zhou M, Mu F, Yan Y, Huang K, Zhao X, Zhang J, Wang S, Gao P and Ou X 2020 *APL Mater.* **8** 051110

[10] Yan Y, Huang K, Zhou H, Zhao X, Li W, Li Z, Yi A, Huang H, Lin J, Zhang S, Zhou M, Xie J, Zeng X, Liu R, Yu W, You T and Ou X 2019 *ACS Appl. Electron. Mater.* **1** 1660

[11] Bruel M 1995 *Electron. Lett.* **31** 1201

[12] Singh R, Radu I, Scholz R, Himcinschi C, Gösele U and Christiansen S H 2006 *J. Lumin.* **121** 379

[13] Bruel M 1996 *Nucl. Instruments Methods Phys. Res. Sect. B Beam Interact. with Mater. Atoms* **108** 313

[14] Tong Q Y and Gösele U M 1999 *Adv. Mater.* **11** 1409

[15] Huang K, Jia Q, You T, Zhang R, Lin J, Zhang S, Zhou M, Zhang B, Yu W, Ou X and Wang X 2017 *Sci. Rep.* **7** 15017

[16] Huang K, Li Z, Yan Y, Zhao X, Li W, You T, Zhang S, Zhou H, Lin J, Xu W, Yi A, Huang H, Zhou M, Yu W, Xie J, Zeng X, Liu R and Ou X 2019 *AIP Adv.* **9** 085001

[17] Lin J, You T, Wang M, Huang K, Zhang S, Jia Q, Zhou M, Yu W, Zhou S, Wang X and Ou X 2018 *Nanotechnology* **29** 504002

[18] Hayashi S, Bruno D and Goorsky M S 2004 *Appl. Phys. Lett.* **85** 236

[19] Chen P, Di Z, Nastasi M, Bruno E, Grimaldi M G, Theodore N D and Lau S S 2008 *Appl. Phys. Lett.* **92** 202107

[20] Singh R, Radu I, Scholz R, Himcinschi C, Gösele U and Christiansen S H 2006 *Semicond. Sci. Technol.* **21** 1311

[21] Biersack J F Z and J P 2008 *SRIM computer code*

[22] Massarani B and Bourgoin J C 1986 *Phys. Rev. B* **34** 2470

[23] Moulet C and Goorsky M S 2012 *Ion Implant.* p. 70

[24] Daghbouj N, Li B S, Karlik M and Declemy A 2019 *Appl. Surf. Sci.* **466** 141

[25] Daghbouj N, Li B S, Callisti M, Sen H S, Karlik M and Polcar T 2019 *Acta Mater.* **181** 160

[26] Nastasi M, Höchbauer T, Lee J K, Misra A, Hirth J P, Ridgway M and Lafford T 2005 *Appl. Phys. Lett.* **86** 154102

[27] Daghbouj N, Li B S, Callisti M, Sen H S, Lin J, Ou X, Karlik M and Polcar T 2020 *Acta Mater.* **188** 609

[28] Luce F P, Reboh S, Vilain E, Madeira F, Barnes J P, Rochat N, Salvetat T, Tauzin A, Milesi F, Mazen F and Deguet C 2014 *IEEE* 2014 20*th International Conference on Ion Implantation Technology (IIT)*, June 26–July 4 2014 Portland, OR, USA p. 1

[29] Daghbouj N, Cherkashin N, Darras F X, Paillard V, Fnaiech M and Claverie A 2016 *J. Appl. Phys.* **119** 135308

[30] Chicoine M, Roorda S, Masut R A and Desjardins P 2003 *J. Appl. Phys.* **94** 6116

[31] Cherkashin N, Daghbouj N, Darras F-X, Fnaiech M and Claverie A 2015 *J. Appl. Phys.* **118** 245301